LA-UR-15-27132
Approved for public release; distribution is unlimited.

Title: Analytical Chemistry and Materials Characterization Results for Debris Recovered from Nitrate Salt Waste Drum S855793

Author(s): Martinez, Patrick Thomas; Chamberlin, Rebecca M.; Schwartz, Daniel S.; Worley, Christopher Gordon; Garduno, Katherine; Lujan, Elmer J. W; Borrego, Andres Patricio; Castro, Alonso; Colletti, Lisa Michelle; Fulwyler, James Brent; Holland, Charlotte S.; Keller, Russell C.; Klundt, Dylan James; Martinez, Alexander; Martin, Frances Louise; Montoya, Dennis Patrick; Myers, Steven Charles; Porterfield, Donivan R.; Schake, Ann Rene; Schappert, Michael Francis; Soderberg, Constance B.; et al.

Intended for: Report

Issued: 2015-09-16 (rev.1)

Analytical Chemistry and Materials Characterization Results for Debris Recovered from Nitrate Salt Waste Drum S855793

Patrick T. Martinez, Rebecca M. Chamberlin, Daniel S. Schwartz, Christopher G. Worley, Katherine Garduno, Elmer J. W. Lujan, Andres P. Borrego, Alonso Castro, Lisa M. Colletti, James B. Fulwyler, Charlotte S. Holland, Russell C. Keller, Dylan J. Klundt, Alexander Martinez, Frances L. Martin, Dennis P. Montoya, Steven C. Myers, Donivan R. Porterfield, Ann R. Schake, Michael F. Schappert, Connie Soderberg, Khalil J. Spencer, Floyd E. Stanley, Mariam R. Thomas, Lisa E. Townsend, Ning Xu

Actinide Analytical Chemistry Group (C-AAC)
Nuclear Materials Science Group (MST-16)
Advanced Nuclear Technology Group (NEN-2)

September 2015

Los Alamos NATIONAL LABORATORY EST.1943

Executive Summary

Solid debris was recovered from the previously-emptied nitrate salt waste drum S855793. The bulk sample was nondestructively assayed for radionuclides in its as-received condition. Three monoliths were selected for further characterization. Two of the monoliths, designated Specimen 1 and 3, consisted primarily of sodium nitrate and lead nitrate, with smaller amounts of lead nitrate oxalate and lead oxide by powder x-ray diffraction. The third monolith, Specimen 2, had a complex composition; lead carbonate was identified as the predominant component, and smaller amounts of nitrate, nitrite and carbonate salts of lead, magnesium and sodium were also identified. Microfocused x-ray fluorescence (MXRF) mapping showed that lead was ubiquitous throughout the cross-sections of Specimens 1 and 2, while heteroelements such as potassium, calcium, chromium, iron, and nickel were found in localized deposits. MXRF examination and destructive analysis of fragments of Specimen 3 showed elevated concentrations of iron, which were broadly distributed through the sample. With the exception of its high iron content and low carbon content, the chemical composition of Specimen 3 was within the ranges of values previously observed in four other nitrate salt samples recovered from emptied waste drums.

1. Subsampling and Non-Destructive Survey of Bulk Radionuclides

Nitrate salt debris was sampled from remnants found in the emptied, previously-remediated waste drum S855793 in August 2014, and the debris was characterized using a suite of analytical tools during the period January-June 2015. The debris is highly heterogeneous in appearance, consisting of moist, red-brown aggregates, and off-white free-flowing solid chunks (Figure 1). A few pieces had dimensions as large as 2 cm, while most were 1 cm or less.

Drum S855793, overpack 69120

Contained 2 gallons of free liquid, pH 0.
Processed December, 2013
Daughters: 68680, 68685

Sampled 8/7/2014
58.25 g solid collected
Heterogeneous, red-brown moist clumps and off-white, free-flowing solid.

Figure 1. General sample description and process history of Drum S855793.

The 58-g bulk solid sample was assayed non-destructively by gamma spectroscopy in its original sample collection container, a screw-cap Teflon jar. Evaluation of the data using SNAP™ gamma spectral analysis code yielded the radionuclide concentrations in Table 1. The uncertainties in Table 1 are related to counting statistics only. Because of the non-ideal geometry of the clumpy debris, the absolute values of the radionuclide concentrations may be collectively biased by 30% or more, but the ratios between nuclides are expected to be accurate within counting uncertainty. Also in Table 1, the non-destructive gamma assay results for four previously-characterized samples of similar nitrate salt debris[1] are provided for comparison. The plutonium, americium and neptunium content all lie at the upper end of the range of previously characterized salt debris samples, while the ^{235}U content is potentially out of the ordinary, at roughly twice the maximum value of the previous samples. The $^{241}Am/^{239}Pu$ and $^{243}Am/^{241}Am$ ratios also fall within values previously recorded for this waste type.

Using microfocused xray fluorescence (MXRF) mapping of the high-atomic weight (>Mg) elements in previous nitrate salt samples, it was observed that off-white pieces of nitrate salt samples were dominated by lead salts, while the more highly colored red-brown pieces had a complex composition including transition metals and lead. A tentative hypothesis was that the off-white pieces had formed after nitric acid dissolution of the lead shielding during drum storage, while the darker pieces were more representative of the original salt composition.

Table 1. Gamma spectroscopic assay of the as-received S855793 sample, compared to other nitrate salt drum debris samples. ND indicates a nuclide was not detected in the 5000-second live time count.

	S855793 69120	**S864694** 69139	**S822952** 68492	**S818449** 68645	**S851436** 69173
Plutonium					
^{238}Pu (µg/g)	ND	ND	3.03e-01	ND	ND
^{239}Pu (µg/g)	5.17e+02 (4%)	9.51e+02	9.26e+01	2.44e+02	6.95e+01
^{240}Pu (µg/g)	2.75e+01 (26%)	5.32e+01	8.94e+00	ND	ND
^{241}Pu (µg/g)	4.03e-01 (14%)	6.84e-01	3.91e-01	1.80e-01	5.42e-02
Americium					
^{241}Am (µg/g)	1.44e+02 (4%)	1.22e+02	1.61e+01	7.86e+01	9.52e00
^{243}Am (µg/g)	3.30e-01 (4%)	2.59e-01	1.94e-04	6.76e-04	3.20e-02
Neptunium					
^{237}Np (µg/g)	5.60e+00 (4%)	5.41e+00	8.83e-01	2.95e+00	3.60e-01
Uranium					
^{235}U (µg/g)	1.16e+02 (6%)	5.89e+01	6.28e+01	6.21e+01	1.68e+01
^{238}U (µg/g)	ND	ND	2.42e+04	4.20e+03	ND
Selected Ratios					
^{241}Am/^{239}Pu (g/g)	0.28	0.13	0.17	0.32	0.14
^{241}Am/^{243}Am (g/g)	440	470	84,000	120,000	300

The salts from drum S855793 contained two medium-sized pieces of off-white material (Specimens 1 and 2), and one large red-brown piece (Specimen 3), which could easily be isolated for semi-quantitative characterization and a test of this hypothesis (Figure 2). Specimen 1 is elongated in shape, while Specimen 2 is a thick plate; both were dry and brittle and easily snapped into two parts at their midlines. Specimen 3 is crumbly and rounded, with a portion of its material loosely adhered to the surface as a result of the sampling process. Specimen 3 did not have enough structural integrity to be cross-sectioned, so loose debris was used for its characterization. The rest of the bulk sample appeared visually similar to Specimen 3, but was not characterized in detail.

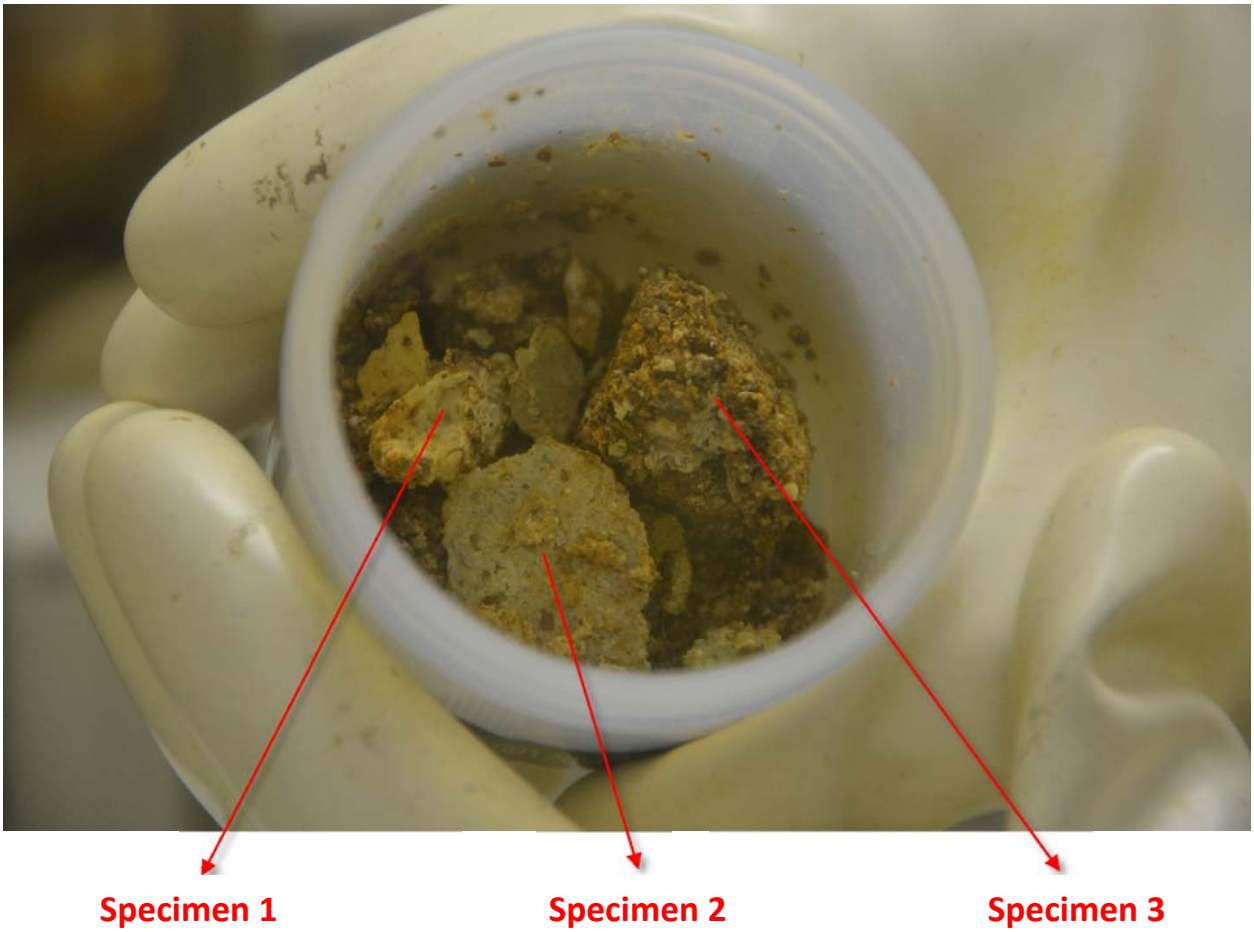

Figure 2. Three larger pieces of salt debris that were isolated for detailed characterization.

Small portions of these specimens were dried at 110 °C and crushed into powder with a mortar and pestle, then individually assayed by gamma spectroscopy for 50,000-60,000 seconds live time. Automated spectral analysis codes gave weak estimates of the Pu concentrations in these samples, so the mass concentrations of the major nuclides ^{239}Pu and ^{241}Am were estimated by manually comparing the 125 and 129 keV spectral peaks, adjusting for branching ratio and efficiency differences). The resulting estimates are provided in Table 2. The radionuclide content of Specimen 3 is most similar to that of the bulk S855793 salt, while Specimen 2 is an order of magnitude lower in concentration. It is

also worth noting, with caution due to the low count rates, that Specimen 2 has a much larger Am/Pu ratio than any of the other nitrate salt samples reported in Table 1.

Table 2. Concentration estimates for major radionuclides in the three salt waste specimens. ^{241}Am concentration was estimated using SNAP™ spectral analysis code (counting uncertainties are 5-6%). The ^{239}Pu values are calculated.

	^{241}Am/^{239}Pu (g/g)	^{241}Am (µg/g)	^{239}Pu (µg/g)
Bulk Sample	0.28	144	517
Specimen 1	0.18	39	216
Specimen 2	0.97	40	41
Specimen 3	0.51	130	254

2. Composition of Solids by Powder X-Ray Diffraction

Representative 1-g portions of the three specimens were dried at 110 °C for 70 hours then crushed for powder x-ray diffraction (XRD) measurement. The weight lost during the drying process (Table 3) represents the mass of volatile components such as water and nitric acid in the salts. The large weight loss observed for Specimen 3 is consistent with qualitative observation that the solid was moist and clumping. Similarly, the more friable nature of Specimens 1 and 2 is consistent with their low water content.

Table 3. Fractional loss of mass (*i.e.* loss-on-ignition) after heating salt specimens to 110 °C.

	% mass change
Specimen 1	6.92 %
Specimen 2	2.15 %
Specimen 3	25.65 %

Each of the specimens contained a number of identifiable crystalline components, in addition to a sizeable non-crystalline portion, which is evidenced by a broad background centered around 22° that tails off by ~30° in the XRD pattern. The primary (P) and secondary (S) crystalline components of the three specimens are identified in Table 4. “Primary” constituents are the one or two compounds whose dominant peaks account for most of the diffraction pattern. All other positively-identified substances are deemed “secondary.” Substances listed in Table 4 are identified in accordance with International Centre for Diffraction Data (ICDD) database nomenclature. Where appropriate, the common chemical name is provided in italics in addition to the ICDD mineral name.

Table 4. Primary (P) and Secondary (S) crystalline components of the three nitrate salt specimens.

	Specimen 1	Specimen 2	Specimen 3
Sodium Compounds			
Nitratine, $NaNO_3$ (*sodium nitrate*)	**P**	S	**P**
Sodium nitrite $NaNO_2$		S	
Sodium nitrate oxide Na_3ONO_2		S	
Magnesium Compounds			
Magnesite, $MgCO_3$ (*magnesium carbonate*)		S	
Lead Compounds			
Lead nitrate, $Pb(NO_3)_2$	**P**	S	**P**
Cerussite, $PbCO_3$ (*lead carbonate*)		**P**	
Lead nitrate oxalate, $Pb_2(NO_3)_2(C_2O_4)$	S		S
Lead oxide, PbO_2	S		S
Shannonite, Pb_2OCO_3 (*lead carbonate oxide*)		S	

Specimen 1 and Specimen 3 are similar in their crystalline content. Both specimens contain mostly nitratine (sodium nitrate, $NaNO_3$) and lead nitrate $Pb(NO_3)_2$. Both also show the presence of lead nitrate oxalate, $Pb_2(NO_3)_2(C_2O_4)$ and lead oxide, PbO_2, in smaller amounts.

The compounds nitratine and lead nitrate account for most of the crystalline content of Specimen 1. The major and minor constituents are indicated by color-coded hash marks in the XRD pattern shown in Figure 3. The sharpness of the peaks associated with lead nitrate oxalate (red markers) suggests that this compound is present in the form of relatively large single crystallites.

The XRD pattern from Specimen 3 is shown in Figure 4; note that diffraction angles up to 60 degrees are displayed, *versus* 100 degrees in Figure 3. It is qualitatively similar to that for Specimen 1, with the same dominance of nitratine and lead nitrate in the mixture. The minor constituents appear to be the same as well. However, Specimen 1 is richer in lead nitrate than Specimen 3, based on relative peak intensities. Their XRD patterns are superimposed in Figure 5. The lead nitrate peaks, indicated by green hash marks, are clearly larger in Specimen 1 (upper white curve), while the peaks for sodium nitrate (nitratine) are comparable in size. No match was found for one peak at ~30°, marked with the green arrow in Fig. 5. It is possible that this is another peak related to lead nitrate oxalate that was not

Compound	ICDD id. no.	Color code
Nitratine $NaNO_3$	00-036-1474	green
Lead nitrate $Pb(NO_3)_2$	01-078-1526	cyan
Lead nitrate oxalate $Pb_2(NO_3)_2(C_2O_4)$	00-054-0875	red
Lead oxide PbO_2	00-050-1430	Yellow

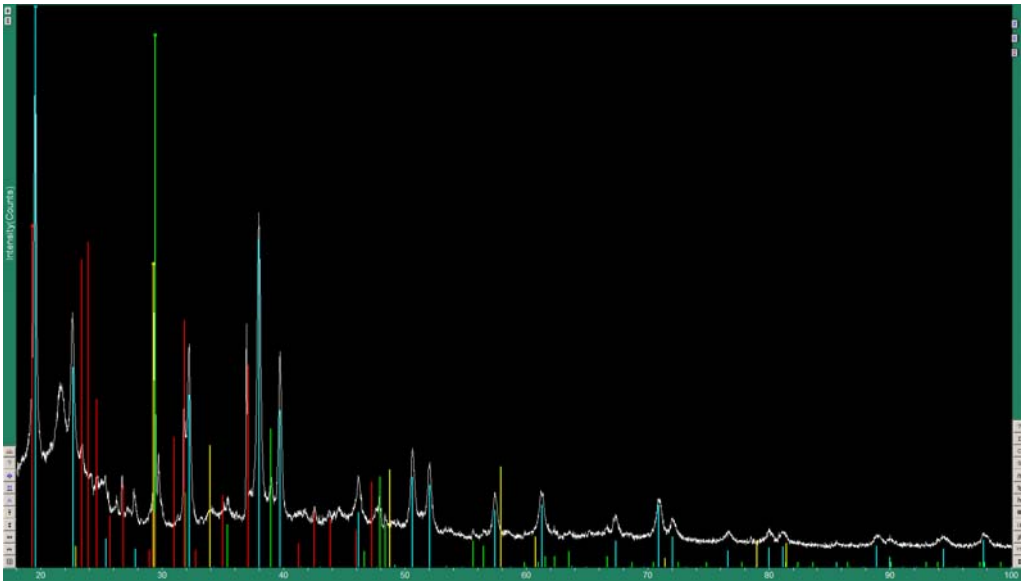

Figure 3. XRD spectrum from Specimen 1. Display axis runs from 20 to 100 degrees diffraction angle.

Compound	ICDD id. no.	Color code
Nitratine $NaNO_3$	00-036-1474	green
Lead nitrate $Pb(NO_3)_2$	01-078-1526	cyan
Lead nitrate oxalate $Pb_2(NO_3)_2(C_2O_4)$	00-054-0875	red
Lead oxide PbO_2	00-050-1430	yellow

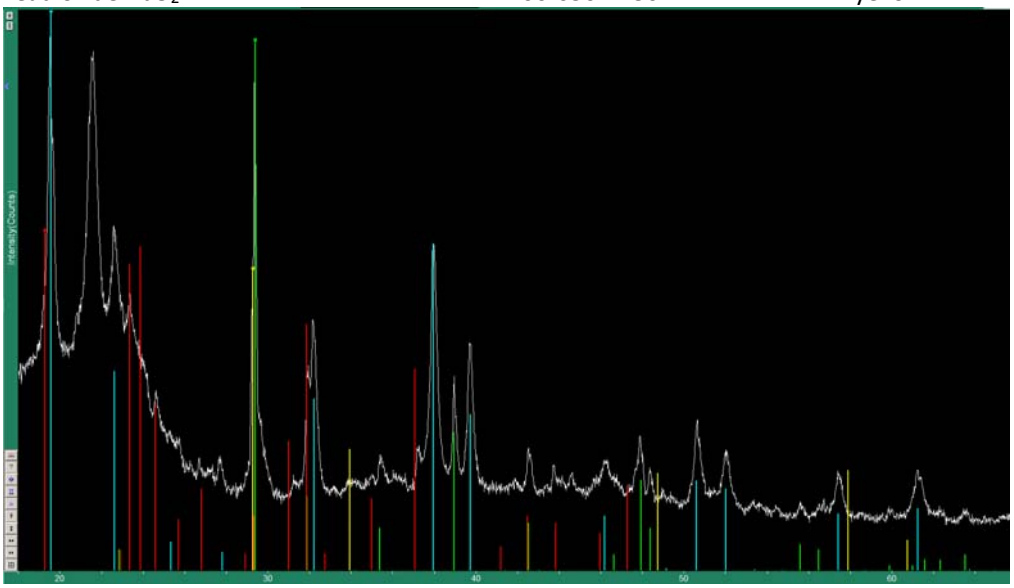

Figure 4. XRD spectrum from Specimen 3. Display axis runs from 20 to 60 degrees diffraction angle.

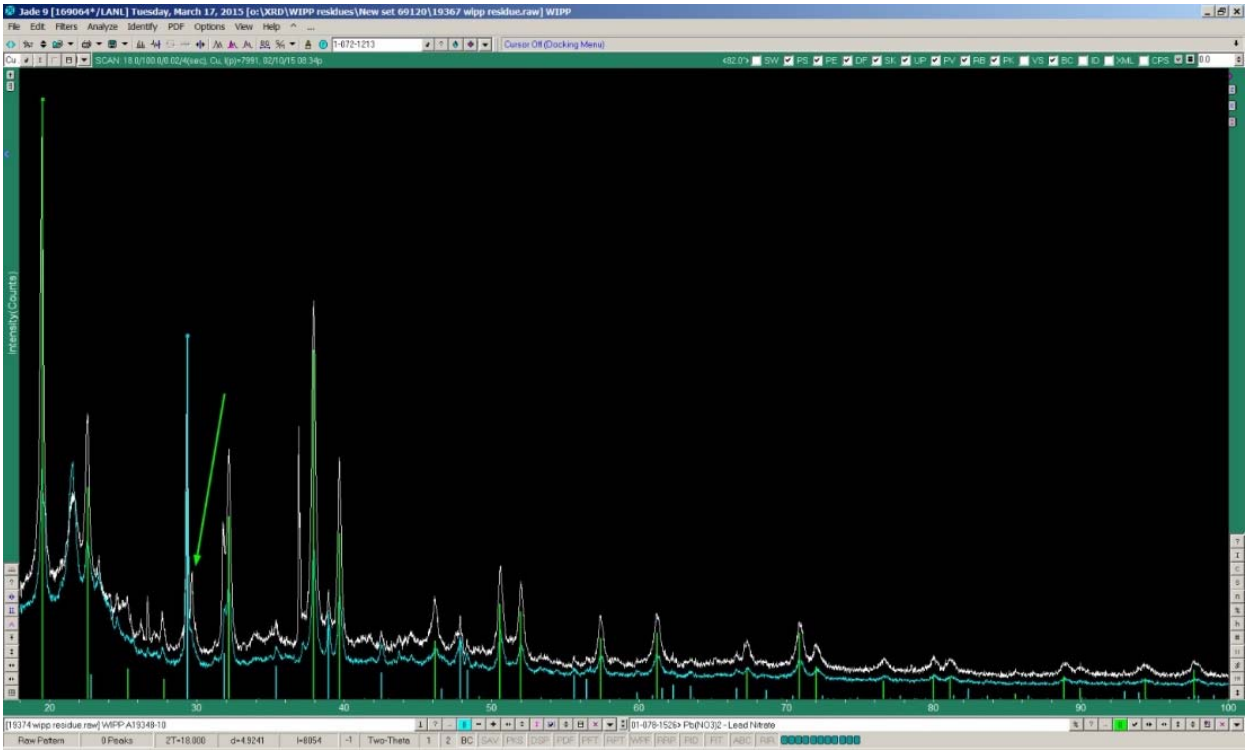

Figure 5. Specimen 1 (white curve) and Specimen 3 (cyan curve) XRD patterns superimposed.

appropriately entered into the ICDD database, as the crystal structure for this compound is very complex.

Specimen 2 is significantly different from the others, showing a large number of small peaks in its XRD spectrum, which indicates that it is a mixture of many compounds. The complex XRD pattern is shown in Figure 6. The list of probable matches is shown below the XRD spectrum, with cerrusite ($PbCO_3$, lead carbonate) accounting for the majority of the content. Sodium nitrite, $NaNO_2$; sodium nitrate oxide, $Na_3O(NO_2)$[2]; nitratine, $NaNO_3$; magnesite, $MgCO_3$; lead nitrate, $Pb(NO_3)_2$; and shannonite $Pb_2O(CO_3)$ were all present in smaller quantities. The upper curve in the XRD pattern shows the spectrum with lines marking all peaks associated with the entire list of probable compounds.

Unlike the other two specimens, lead nitrate and nitratine were present only in small amounts in Specimen 2. Instead, the dominant crystalline component is cerussite, $PbCO_3$. The identification of a dominant carbonate salt is unexpected, because the nitrate salt wastes originated from evaporation of acidic solutions, where carbonate ion is not expected to be stable. It is possible that the carbonate arose from thermal or radiolytic decomposition of oxalic acid or metal oxalates, but the absence of any crystalline oxalates in the XRD makes this difficult to verify. Lead carbonate had also been identified in the XRD pattern of residues from nitrate salt drum S851436[1], which contained visually similar off-white plate-like solids.

Compound	ICDD id. no.	Color code
Cerussite $PbCO_3$	01-070-2052	green
Sodium nitrite $NaNO_2$	01-089-2830	cyan
Sodium nitrate oxide Na_3ONO_2	01-070-0132	red
Nitratine $NaNO_3$	01-072-1213	magenta
Magnesite $MgCO_3$	01-086-0175	yellow
Lead nitrate $Pb(NO_3)_2$	01-071-3821	purple
Shannonite Pb_2OCO_3	01-071-6312	green

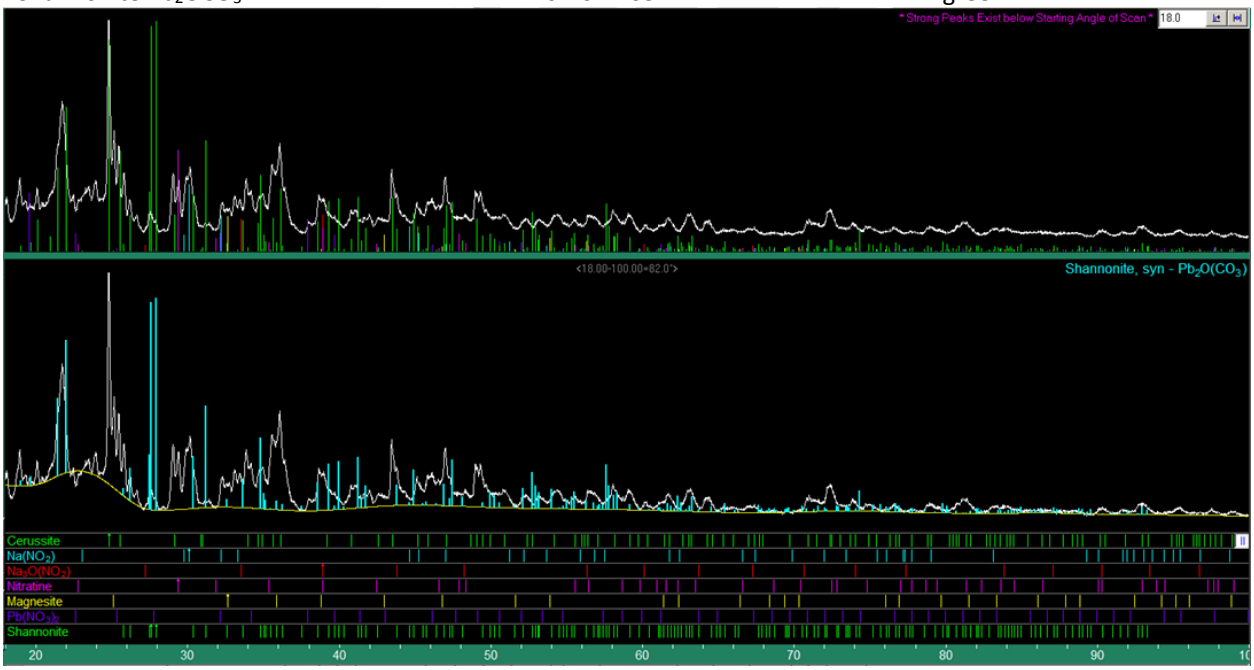

Figure 6. XRD spectrum from Specimen 2. Display axis runs from 20 to 100 degrees diffraction angle

3. Verification of Nitrite (NO_2^-) by Anion Chromatography

Nitrite anion (NO_2^-), which was identified in one of the mineral phases of Specimen 2, is a redox agent in some plutonium recovery processes and can arise from alpha and gamma radiolysis of nitrate-containing solids and solutions. Since its potential for promoting reactivity with organic compounds in nitric acid media is well-established, portions of all three monoliths from S855793 were analyzed by anion chromatography to verify and quantify the presence of nitrite. The results are presented in Table 5. Nitrite is indeed more abundant in Specimen 2 than the others, both in its absolute concentration (about 3 times greater) and in proportion to the dominant nitrate ion (1:26 *versus* 1:350).

Other anions confirmed in the specimens include fluoride, chloride, and oxalate. Carbonate cannot be quantified in the buffer system used in this analysis, and the oxalate measurement detects only free oxalate ion, not metal oxalates.

Table 5. Nitrite and other anions in Specimens 1-3 (µg/g as-received salt).

	Specimen 1	Specimen 2	Specimen 3
NO_2^-, nitrite (µg/g)	**770**	**2250**	**650**
NO_3^-, nitrate (µg/g)	**268,000**	**59,000**	**223,000**
NO_3^- / NO_2^- ratio	**348**	**26**	**343**
F^-, fluoride (µg/g)	210	130	650
Cl^- chloride (µg/g)	470	1290	750
$C_2O_4^{2-}$, oxalate (soluble, µg/g)	1960	210	820

4. Elemental Composition and Distribution by Microfocused X-Ray Fluorescence

Spatially-resolved x-ray fluorescence spectroscopy using a microfocused excitation beam provides semi-quantitative information about the presence and distribution of elements heavier than Mg. For this study, cross-sectioned Specimens 1 and 2 were mounted between two pieces of foam with the relatively flat side of the broken surface facing up to be analyzed. The specimens were sealed inside a plastic cup with 4 µm Prolene film. Fragments of Specimen 3 were collected on clear tape and sealed inside a plastic cup with 6 µm Mylar film. While the lack of cleanly-cut, flat surfaces in these samples makes it difficult to infer concentration gradients from small intensity differences, careful examination of the spectral peaks from more prominent spots supports the conclusions that are presented in this section.

The composite visible light image of Specimen 1 in Figure 7 shows the method of sample mounting and the rough, porous surface texture. The red boxed area in the enlarged image at right was imaged by MXRF (3.7 mm x 2.9 mm). Only a small portion of the edge could be focused for analysis with the x-ray beam. Figure 8 shows the important elemental maps for this specimen.

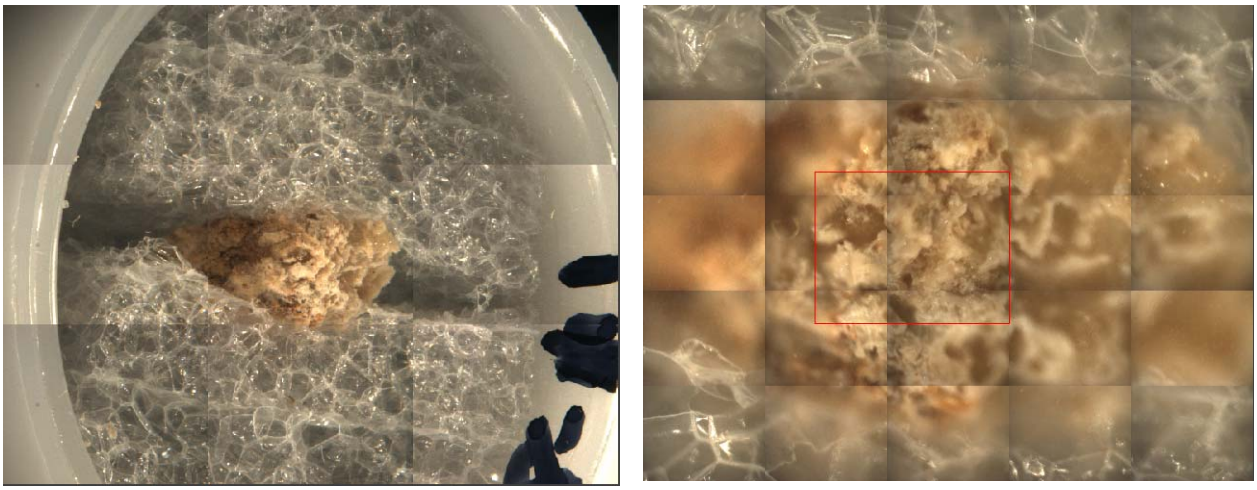

Figure 7. Specimen 1, sectioned and mounted for MXRF analysis. The red box denotes the imaged area.

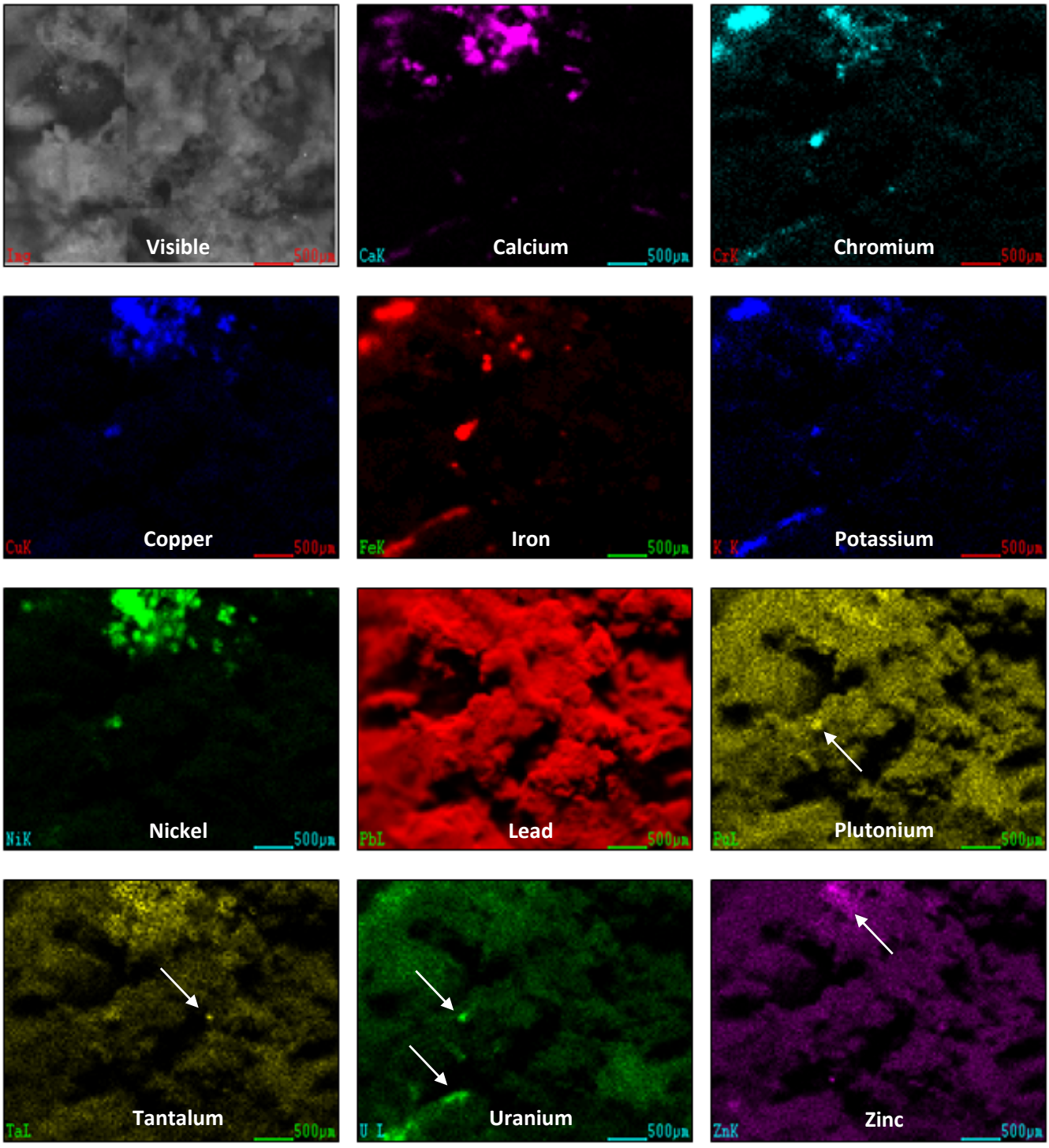

Figure 8. Notable MXRF elemental images collected from a 3.7 mm x 2.9 mm area of Specimen 1.

At top left of Figure 8 is the visible image for reference. Lead was ubiquitous throughout the cross-sectioned surface (3rd row center); the dark areas in the image correspond to surface pores. Considerable calcium, copper and nickel deposits were localized in the top center of the imaged area. Chromium, iron, potassium, uranium and zinc also occurred together in specific regions. The Pu image (3rd row right) mostly arises from background scatter, but the spot left of middle does appear to contain more Pu than surrounding areas.

Figures 9 and 10 provide additional visualization tools for some complex areas of the images. The six-color image in Figure 9 shows the dominant elemental signal per pixel among the six elements calcium, chromium, copper, iron, nickel and lead. Figure 10 is a three-color overlay of the nickel (red), iron (green), and chromium (blue) element maps. The top center red area contains mostly nickel. The white

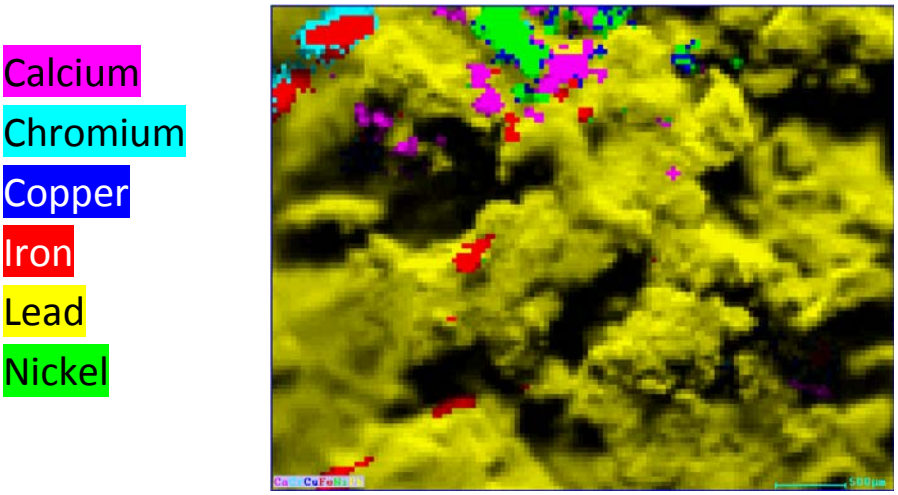

Figure 9. Dominant elemental signal per pixel in Specimen 1, of the six elements displayed.

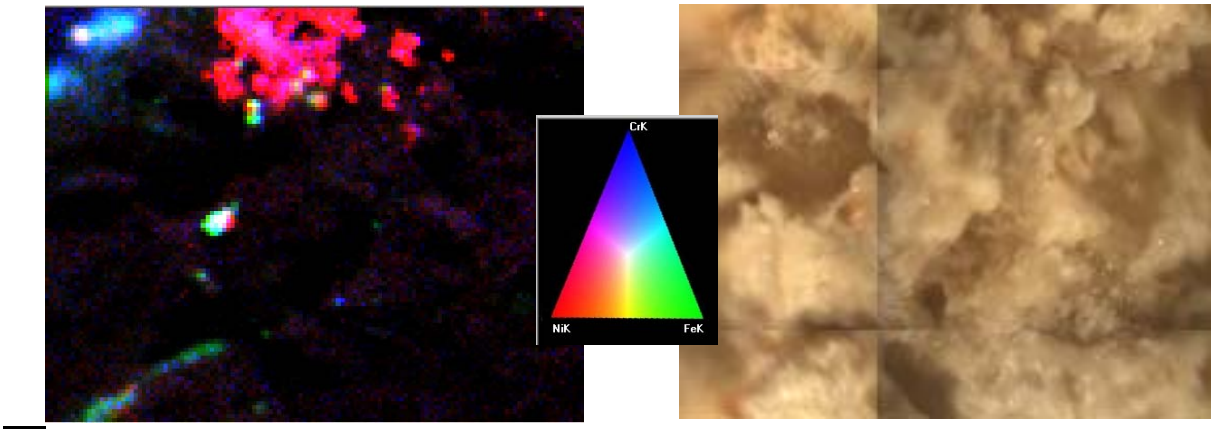

Figure 10. Overlaid nickel (red), iron (green), and chromium (blue) maps for Specimen 1 at left, and visible light image at right.

spots, left of center and just below the red area, contain substantial amounts of all three elements (probably a piece of steel) and correspond to dark inclusions at left of center in the visible image.

Specimen 2 was similarly mounted and a 4.5 mm x 3.5 mm. area was selected for MXRF analysis (Figure 11). The visible light images of the cross-section show some pores or cavities. Elemental maps for Specimen 2 are presented in Figure 12. Lead is again shown to be ubiquitous throughout the sample, and evenly deposited. The crevices in the specimen appear dark because they do not reside in the focal plane, and because any signal emitted could not reach the detector. Other notable elemental maps include copper, iron, potassium, nickel and uranium. A trace amount of Pu was detected, but the Pu image (not shown) displayed mostly background scatter.

Figure 13 is an overlay of the nickel (red), iron (green), and uranium (blue) images. There is not much iron and nickel overlap (yellow) in this cross-section, but inclusions that contain uranium along with nickel and/or iron are visible as magenta, cyan, and white spots.

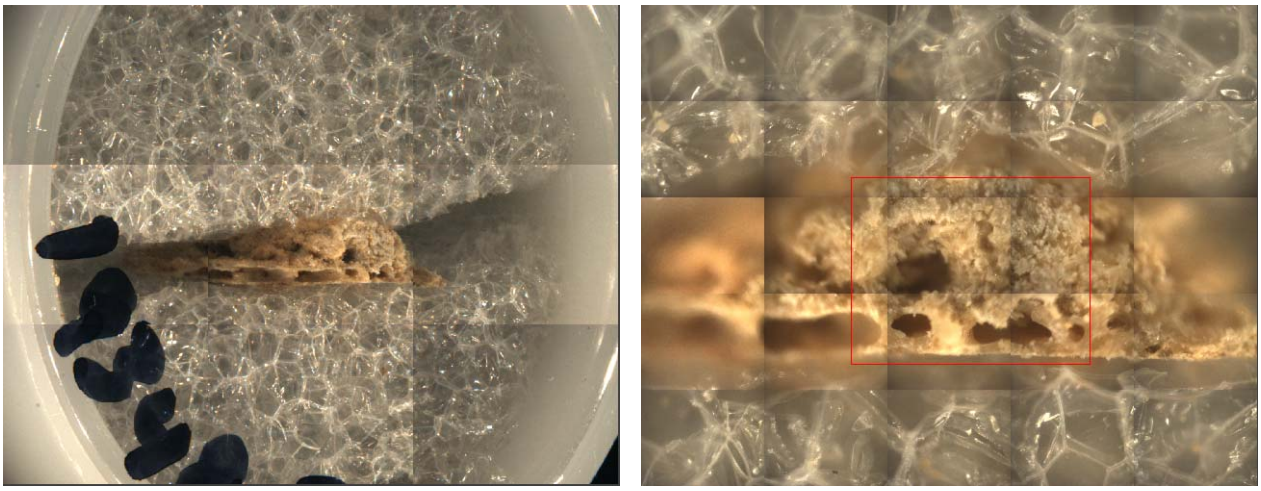

Figure 11. Specimen 2, sectioned and mounted for MXRF analysis. The red box denotes the imaged area.

Combined, these MXRF observations for Specimens 1 and 2 illustrate that the lead compounds that were identified in the x-ray diffractions studies were not deposited onto the exterior surfaces of nitrate salt monoliths. Rather, the uniform deposition of lead throughout the cross-section of Specimen 1 suggests that a lead-containing solution suffused throughout the sodium salt, scavenging anions to form lead nitrate and lead nitrate oxalate. Specimen 2, which contains mostly lead carbonate and smaller amounts of nitrate, has a similarly uniform deposition of lead. This material may have precipitated gradually as carbonate ions were generated within the drum and scavenged by lead and magnesium.

Both samples also displayed localized hot-spots of heteroelements such as iron, nickel, chromium, and uranium. These are more widely distributed throughout the cross-section of Specimen 2 than 1.

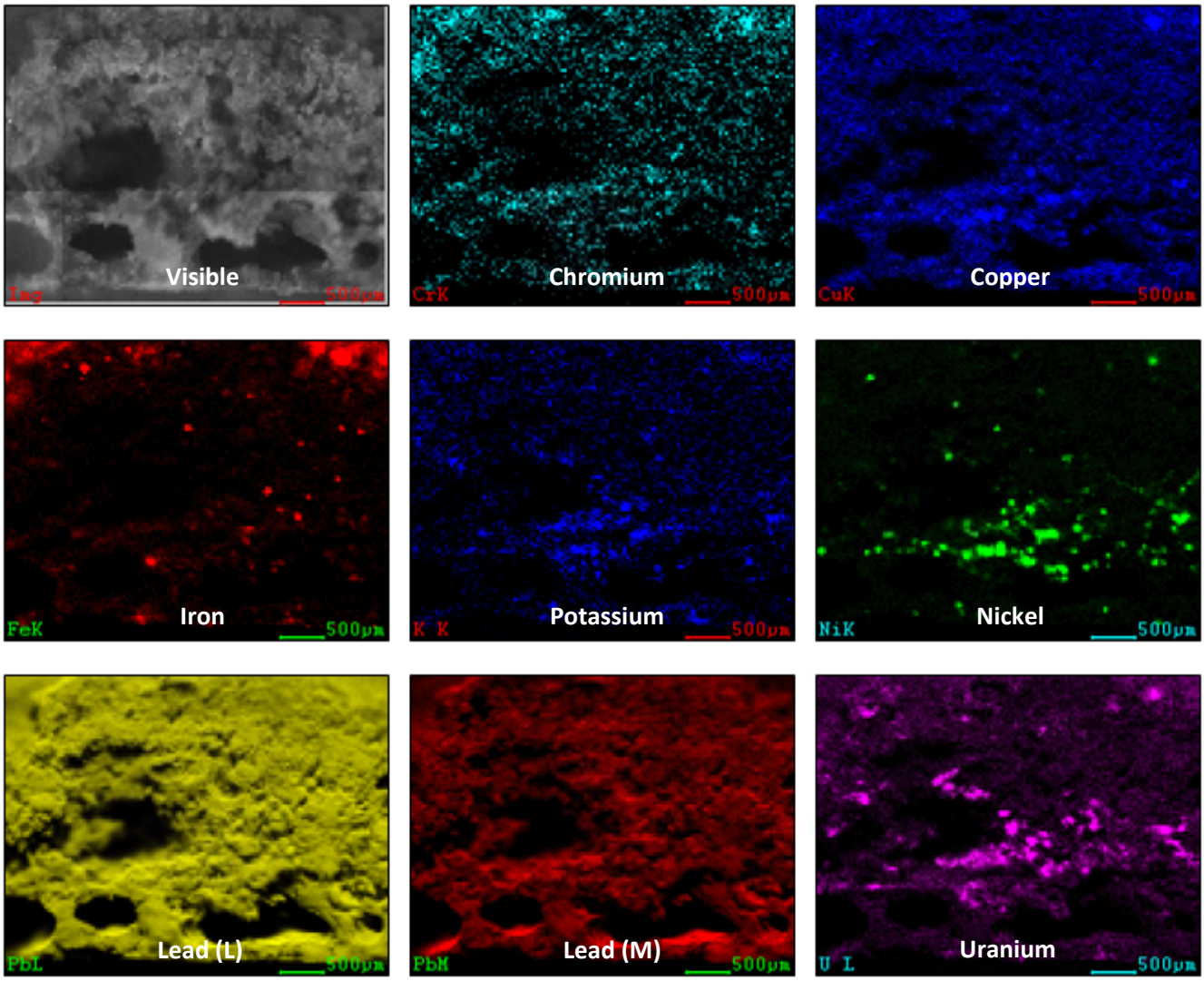

Figure 12. Notable MXRF elemental images collected from a 4.5 mm x 3.5 mm area of Specimen 2.

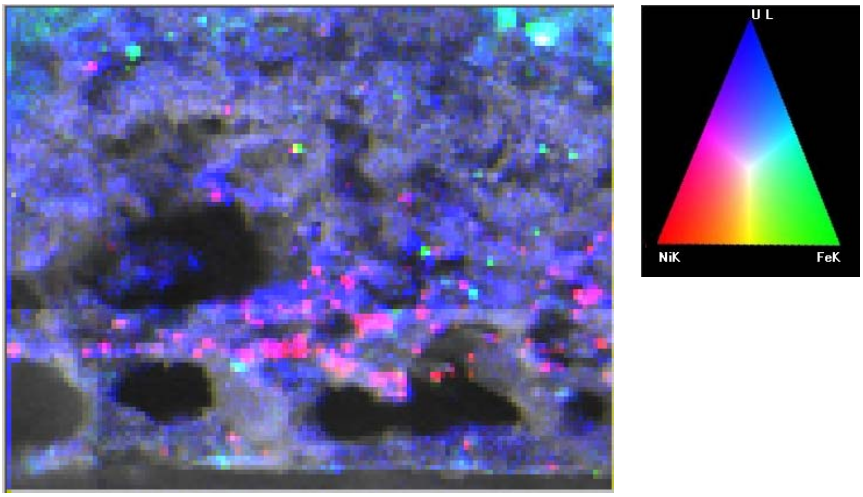

Figure 13. Overlay of nickel (red), iron (green), and uranium (blue) in Specimen 2.

Specimen 3 was more friable, so the MXRF characterization was performed by affixing a collection of its small fragments onto tape (Figure 14). Imaging was performed over the 7.5 mm x 5.9 mm area identified by the red box in Figure 14. Elemental maps are shown in Figures 15 and 16. The six-color image in Figure 15 shows the dominant signal per pixel among the six elements chromium, iron, lead, plutonium, uranium, and zinc, and individual element maps are presented in Figure 16. Nearly all of the particles appeared to have high lead content, a possible exception being the large particle at far right that is displayed in cyan (uranium) and blue (chromium) in the six-color image (Figure 15). A similar cyan (uranium) fragment appears at the top edge of Figure 15, just right of center. Both of these fragments are dark on the lead element map in Figure 16, indicating either that their lead content is low, or that other elements are deposited on the surface of the particle. Iron-containing particles are also ubiquitous in this specimen, an unusual occurrence compared to other nitrate salt wastes.

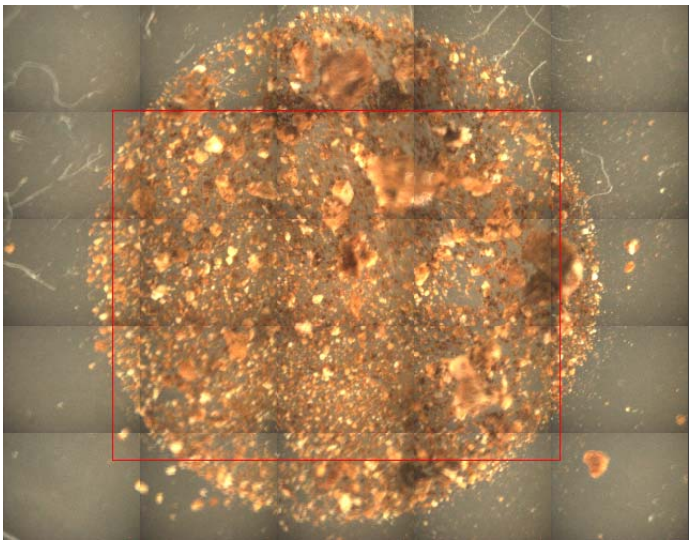

Figure 14. Broken pieces from Specimen 3 mounted for MXRF analysis.

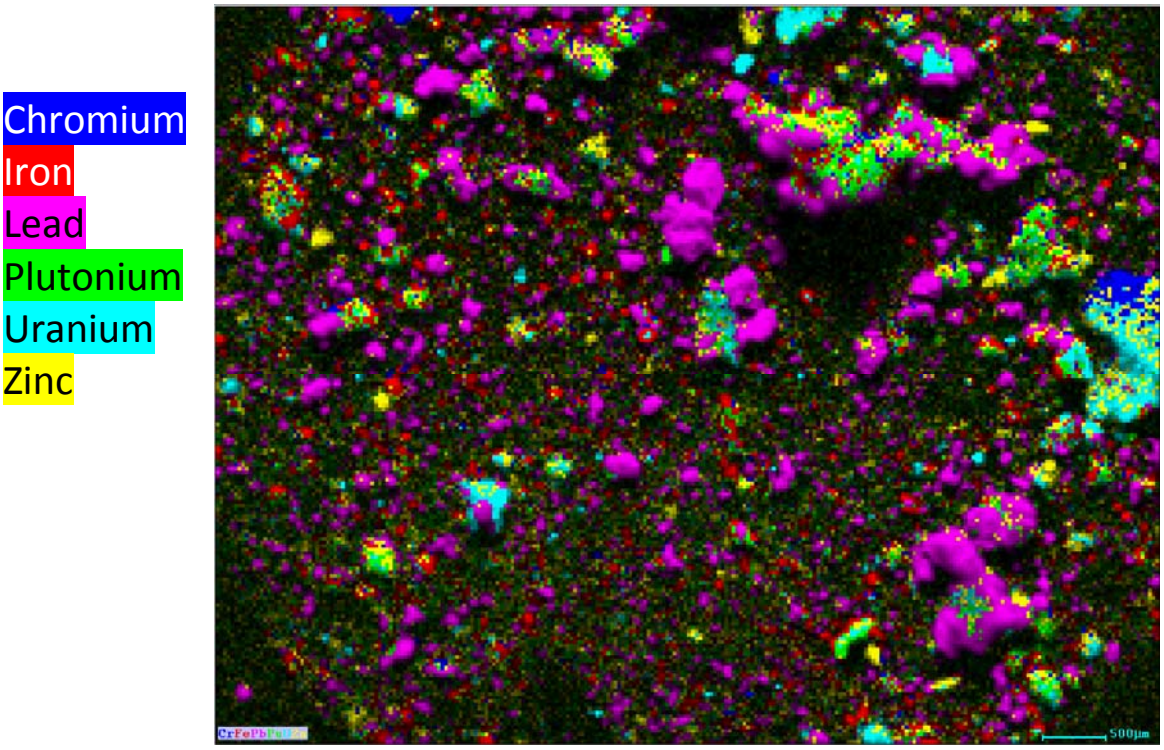

Figure 15. Dominant elemental signal per pixel in Specimen 1, of the six elements displayed.

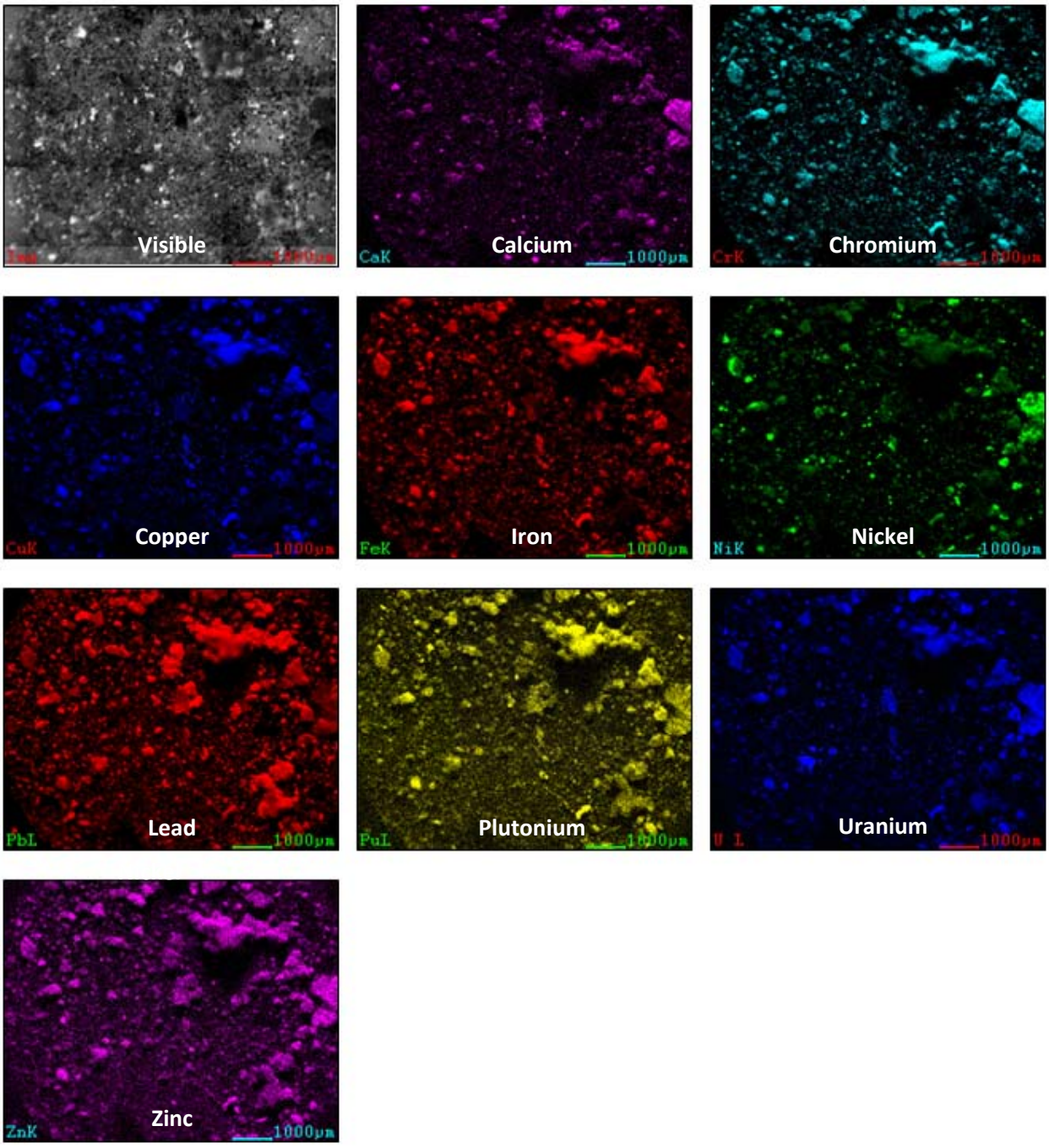

Figure 16. Notable MXRF elemental images collected from a 7.5 mm x 5.9 mm area of Specimen 3. Some of the plutonium features result from high spectral background associated with the lead.

5. Destructive Analysis of Specimen 3

To obtain a complete compositional profile of Specimen 3, three pretreatment pathways were used to support eight categories of analysis. The first two of these, XRD and MXRF analysis, have already been described in the preceding sections. Further details of the methods are available in Reference 1.

1) Intact solid (dried at 110 °C)
    a. X-ray diffraction for bulk phases
    b. Microfocused x-ray fluorescence for elemental distribution
    c. Carbon analysis by combustion

2) Water extraction (ambient temperature)
    a. pH measurement and H^+ titration
    b. Anion analysis by ion chromatography

3) Acid digestion, after ashing at 600 °C
    a. Metals quantification by ICP-AES and ICP-MS
    b. Plutonium quantification and isotopics by Isotope Dilution TIMS
    c. Qualitative characterization of undigested residue

The composition profile in Figure 17 is a summary view of the percent abundance by mass of the major constituents of the sample. The blue bars represent the mass contribution of each fraction, and the red line shows the cumulative accounting for the overall sample composition. The six segments of the profile are:

Weight Loss (<110 °C) is the mass change in the sample after drying at 110 °C. This loss-on-ignition fraction represents 22.9% of the sample mass, and includes any volatile components, primarily loosely-bound water.

Weight Loss (110-600 °C) is the mass change in the sample that occurred after taking the dried sample to 600 °C for complete ashing. At this temperature, combustion of polymers and decomposition of metal oxalates and nitrates has taken place. This high temperature fraction represents 32.8% of the sample.

Nitrates is the mass of nitrate anion (NO_3^-) measured directly by anion chromatography. Nitrate makes up 22.3% of the mass of Specimen 3.

Nitrate Decomposition: A negative mass correction to account for the duplicative reporting of nitrate in the *Weight Loss* and *Nitrates* fractions. Metal nitrates thermally decompose with release of gases, *e.g.* for lead nitrate: $2\ Pb(NO_3)_2\ (s) \rightarrow 2\ PbO\ (s) + 4\ NO_2\ (g) + O_2\ (g)$**.** This decomposition correction is -19.4% for Specimen 3.

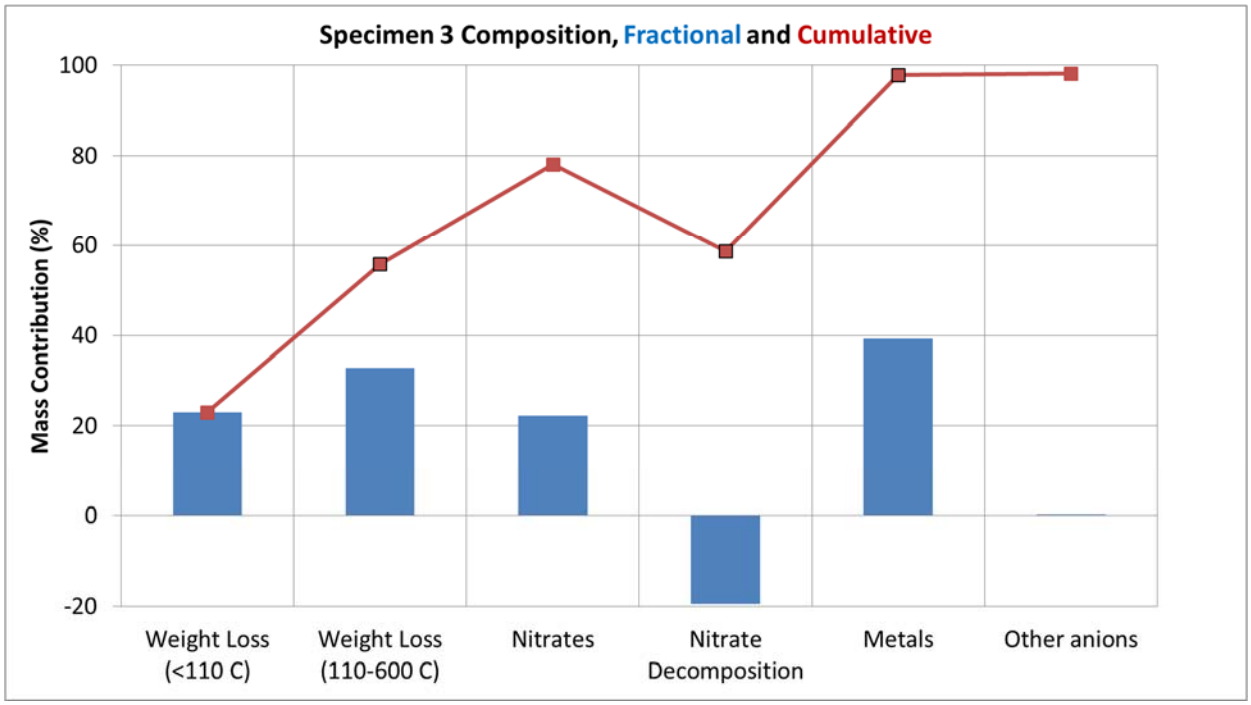

Figure 17. The composition of Specimen 3 is presented in terms of its major components. Fractional mass contributions are shown as blue bars, and the cumulative composition is tallied by the red line. Mass fractions are described in more detail in the text.

Metals includes the mass contribution of all metals measured by ICP-MS and ICP-AES, and reported in Table 6. The metals fraction of Specimen 3 is 39.2%, with lead contributing 30.8%.

Other Anions represents the sum of the other water-soluble anions measured in the sample; any contributions from metal oxides were not directly measured are not included in the composition profile. Other anions contributed 0.3% to the sample mass.

Collectively, this suite of measurements accounted for 98.1% of the Specimen 3 composition. The small remaining mass is most likely attributable to oxygen. Carbonates and metal-bound oxalates in the sample are not directly measured, but their decomposition products (CO, CO_2) are accounted for in the 600 °C weight loss. Similarly, oxygen present as metal oxide would not be detected in these analyses. Additionally, a small portion of the solid was not digested by nitric acid. This residue contained fine particles of tantalum and platinum (by MXRF).

Destructive analysis results for metals and non-metals in the sample are presented in Tables 6 and 7, respectively. Metals analysis was conducted by inductively-coupled plasma atomic emission spectroscopy (ICP-AES) and mass spectrometry (ICP-MS). Plutonium was assayed by thermal ionization mass spectrometry using the isotope dilution technique; plutonium isotopic ratios were also obtained in this analysis (Table 8). The pH associated with the free liquid content in Specimen 3 was determined by titration of the water-extracted sample, and normalized to the as-received sample mass using the 110 °C

Table 6. Metals in Specimen 3 compared to bulk sample characteristics of four other nitrate salts[1]. Additional elements observed at <200 ppm were: Mo (180), B (100), and Zn, Mn, Ti, W at less than 50 ppm each.

	S855793 Specimen 3	**S864694** bulk	**S822952** bulk	**S818449** bulk	**S851436** bulk
Lead (Pb, wt%)	30.8 %	24.2	21.7	18.9	42.0
Sodium (Na, wt%)	3.08 %	3.72	2.73	1.61	1.39
Magnesium (Mg, wt%)	0.59 %	0.21	0.18	3.28	0.74
Aluminum (Al, wt%)	0.70 %	0.60	0.33	2.12	0.38
Calcium (Ca, wt%)	0.26 %	0.25	0.26	0.27	0.16
Iron (Fe, wt%)	1.54 %	0.54	0.28	0.27	0.05
Chromium (Cr, µg/g)	900 µg/g	850	540	410	70
Copper (Cu, µg/g)	380 µg/g	340	200	200	< 8
Gallium (Ga, µg/g)	290 µg/g	490	160	470	190
Nickel (Ni, µg/g)	300 µg/g	730	53	120	30
Potassium (K, µg/g)	3400 µg/g	360	2700	840	65
Uranium (U, µg/g)	2800 µg/g	620	17,300	1900	310
Plutonium (Pu, µg/g)	1160 µg/g	496	83	96	41

Table 7. Non-metals content in as-received Specimen 3, and comparison to bulk sample characteristics of four other nitrate salts[1].

	S855793 Specimen 3	**S864694** bulk	**S822952** bulk	**S818449** bulk	**S851436** bulk
pH, absorbed liquid	2.6	1.8	1.6	2.5	1.7
Carbon (C, wt%)	5.2 %	8.8	9.2	7.2	9.9
Nitrate (NO_3^-, wt%)	22.3 %	21.4	21.8	19.1	14.6
Nitrite (NO_2^-, µg/g)	650 µg/g	600	50	640	70
Fluoride (F^-, µg/g)	650 µg/g	70	1200	12	150
Chloride (Cl^-, µg/g)	750 µg/g	850	380	410	200
Oxalate (soluble, µg/g)	820 µg/g	1400	2800	170	740

Table 8. Plutonium isotopic distribution of Specimen 3.

	S855793 Specimen 3
^{238}Pu, atom%	0.02 %
^{239}Pu, atom%	92.63 %
^{240}Pu, atom%	7.13 %
^{241}Pu, atom%	0.10 %
^{242}Pu, atom%	0.12 %

weight-loss measurement. Carbon was determined by combustion analysis on the dried sample, and anions were determined in the water-extracted sample.

Compared to previously-characterized nitrate salt drum residues, nearly all of the constituents fall within the bounds of typical compositions. However, iron is about 3 times more abundant in Specimen 3 than the highest values previously recorded (1.54 wt% *versus* 0.54 wt%), which is consistent with its prevalence by MXRF. Conversely, carbon is 25-50% lower in this salt monolith than any previously recorded values measured on loose nitrate salt debris.

Finally, in Table 9, the destructive analysis results obtained by LANL for Specimen 3 are compared to the ICP-AES/MS results reported by the DOE Technical Assessment Team (TAT) for a related sample of drum S855793 salts, collected on the same date[3]. While there is little reason to expect identical chemistry between two samples of highly heterogeneous debris, the metal content is in general agreement except for the divergent lead values, and may suggest a common origin at the evaporator processing step. Without a comprehensive accounting of the TAT sample composition (e.g. moisture content), this conclusion remains preliminary.

Table 9. LANL metals analysis results for Specimen 3, compared to results reported by the DOE Technical Assistance Team for a second specimen from the same drum.

	Specimen 3 LANL	**S855793** DOE TAT
Lead (Pb)	30.8 %	11.7 %
Sodium (Na)	3.08 %	2.8 %
Magnesium (Mg)	0.59 %	0.50 %
Aluminum (Al)	0.70 %	0.91 %
Calcium (Ca)	0.26 %	0.05 %
Iron (Fe)	1.54 %	0.73 %
Chromium (Cr)	900 ppm	843 ppm
Copper (Cu)	380 ppm	290 ppm
Gallium (Ga)	290 ppm	--
Nickel (Ni)	300 ppm	343 ppm
Potassium (K)	3400 ppm	1270 ppm
Uranium (U)	2800 ppm	3450 ppm

Notes

[1] "Analytical Chemistry and Materials Characterization Results for Debris Recovered from Four Nitrate Salt Waste Drums," Patrick T. Martinez, Rebecca M. Chamberlin, *et al.*, Los Alamos National Laboratory Report LA-UR-15-26850, September 1, 2015.

[2] While the molecular formula Na_3ONO_2 suggests the crystalline phase contains nitrite anion, the compound is identified as sodium nitrate oxide in the ICDD and in all references cited therein.

[3] "Waste Isolation Pilot Plant Technical Assessment Team Report," D. L. Wilson, *et al.* March 17, 2015 SRNL-RP-2014-01198, March 17, 2015 (Revision 0).